Fire as carbon sink? The global biome-dependent wildfire carbon balance

Simon Bowring (simon_bowring@hotmail.com)
University of Zurich
Matthew Jones
University of East Anglia https://orcid.org/0000-0003-3480-7980
Philippe Ciais
Laboratoire des Sciences du Climat et de l'Environnement https://orcid.org/0000-0001-8560-4943
Bertrand Guenet
Ecole Normal Superieure (Paris)
Samuel Abiven
Ecole Normal Superieure (Paris)

Article

Keywords: wildfire, carbon balance, carbon sink

Posted Date: December 30th, 2020

DOI: https://doi.org/10.21203/rs.3.rs-127629/v1

Version of Record: A version of this preprint was published at Nature Geoscience on February 10th, 2022.
See the published version at https://doi.org/10.1038/s41561-021-00892-0.

Fire as carbon sink? The global biome-dependent wildfire carbon balance

Authors: Simon P.K. Bowring[*,1,2], Matthew W. Jones[3], Philippe Ciais[4], Bertrand Guenet[2], Samuel Abiven[2,5]

Affiliations:

1. Soil science and biogeochemistry group, Department of Geography, University of Zurich, Winterthurerstrasse 190, CH-8057 Zurich, Switzerland
2. Laboratoire de Géologie,Département de Géosciences, Ecole normale supérieure (ENS), 24 rue Lhomond, 75231 Paris Cedex 05, France
3. Tyndall Centre for Climate Change Research, School of Environmental Sciences, University of East Anglia, Norwich, UK
4. Laboratoire des Sciences du Climat et de l'Environnement (LSCE), IPSL, CEA/CNRS/UVSQ, Gif sur Yvette, France
5. *CEREEP-Ecotron IleDeFrance*, CNRS / ENS - UMS 3194, 11 chemin de busseau, 77140 St-Pierre-lès-Nemours, France

Abstract

Wildfires generally result in biospheric recovery approximating the pre-disturbance state. However legacy carbon(C) gains and losses that have until now been overlooked in global-scale theory and modelling indicate that post-fire C gains through pyrogenic carbon (PyC) production, and losses via fire regime shifts, post-fire mortality, topsoil loss and inland water export, may be central to whether 20th century fires have imposed a net terrestrial C source or sink. Here, we integrate PyC production and soil accumulation into a global terrestrial model (ORCHIDEE-MICT) and estimate wildfire C-gains and losses over 1901-2010, quantifying the fire-C balance at global, regional and vegetation scales. Excluding the effect of PyC mineralisation, fires provide a land storage of +177 TgC yr^{-1} (63% PyC production), dominated by grasslands. The global balance is nuanced, with forest fires resulting in strong terrestrial net C loss:gain ratios (>-2:1) that are greatest in tropical regions (>-3:1). Frequent tropical grassland fires are responsible for the bulk of the land PyC sink and its environmental persistence, whose theoretical minimum mean residence time we quantify at 2760yrs. We highlight the dependency of the global fire-C balance on vegetation coverage and the potential role of preserving grasslands, particularly those in the tropics, in that regard.

Wildfires are a key driver of disturbance-recovery cycles in many regions of the world. While fires emit large quantities of C to the atmosphere (~2 PgC yr^{-1})[1], subsequent vegetation recovery re-captures the emitted C on decadal timescales and results in an uncertain but likely small net impact on atmospheric C in the long run. Natural shifts in fire regimes and vegetation occur infrequently and are largely driven by climatic and human perturbations, such that biomes tend towards quasi- steady state outside of these. It is thus assumed that on decadal to centennial time-, and biome to global spatial- scales:

$$E^{-}_{FCO_2} = U^{+}_{VCO_2} \qquad (1)$$

Where E_{FCO_2} is fire CO_2 emissions due to vegetation combustion, and U_{VCO_2} is uptake of atmospheric CO_2 by post-fire vegetation recovery, poles referring to flux direction with respect to C stocks in the terrestrial biosphere.However, recent research on both sides of the flux complicates this perspective. A range of long-term 'legacy' C fluxes traced back to source fire events lead to either C accumulation or loss by land ecosystems, however their balance is yet

to be determined. On the 'legacy sink' side, the charring of biomass by fire creates a by-product known as pyrogenic C (PyC) (~10-20% annual fire CO_2 emissions)[2,3] which is significantly more resistant to biochemical oxidation than bulk soil organic carbon (SOC)[4–6]. Most studies find that PyC degrades with a 'mean residence time' (MRT) of 100s to 1000s of years [7–10] (1-2 orders of magnitude higher than non-PyC SOC), suggesting a sequestration flux from the atmosphere which exceeds the temporal boundaries of the fire-recovery cycle in most fire regimes, driving long-term terrestrial PyC accumulation (SOC^{+}_{PyC}). Of the PyC produced, we assume a fraction additional to SOC^{+}_{PyC} consists of a lightweight 'labile' component that is likewise readily mobilised, hereafter denoted PyC^{+}_{LW} (Supplementary Text S2).

The magnitude of the global PyC sink is dependent on its production rate and MRT with respect to degradation processes, which is a positive function of maximum flame intensitiesy[4,9] related to biomass loading and moisture content[11].

Thus, frequently-burned biomes like grasslands can be expected to host low-intensity fires that produce relatively labile PyC compared to that of forests which host less frequent and more intense fires due to lower and generally wetter fuel stocks. A trade-off between PyC input and MRT determines PyC storage across biomes: Increasing grass cover leads to more frequent PyC production, however this PyC tends to be relatively labile (Fig. 1).

On the 'legacy source' side, fires impose long term C deficits on the terrestrial biosphere via several mechanisms: First, the return of biomes to their pre-fire biomass state (Fig.1a) requires a stable fire regime, in which the biomass recovery interval (BRI; the time period of complete vegetation recovery) is shorter than the fire return interval (FRI; the time between fires). Violation of this condition (BRI < FRI) entails a change in the fire regime and an overall C-deficit, representing a step-wise decrease in biomass C ($VC_{\Delta FiReg}$) and land coverage (Fig. 1a). Second, tropical rainforests exposed to pre-fire disturbances such as drought[12] are vulnerable to episodes of aboveground vegetation-C (VC) mortality (VC_{Mort}) in the decades following fires (VC_{Mort} can exceed 25% of VC)[13,14]. Third, in areas where the existing fire regime results in higher fire frequencies than the average for that vegetation type, large fractions of SOC can be lost through combustion, erosion and microbial mineralisation (SOC_{hfloss}). Topsoil SOC losses through this mechanism have been observed to exceed 20% on average in grasslands and broadleaf forests[15]. Fourth, PyC is liable to export from land to oceans via rivers (SOC^{-}_{PyCExp}) in particulate or dissolved form (Py-POC; Py-DOC, respectively), totalling >40 TgPyC-C yr^{-1} [7,16]. A fraction of this exported PyC is later deposited to the ocean floor up to 1E+04 yrs[7] after its initial production, with some proportion of photo-oxidative degradation occurring en route[17]. Although considered as a loss term in the terrestrial C budget equation below, SOC^{-}_{PyCExp} largely represents C displacement from terrestrial to aquatic realms, not an atmospheric flux. Finally, substantial amounts of PyC are lost through mineralisation in soils and inland aquatic systems (E_{PyC})[17], though this quantity is poorly constrained in part due to the challenges surrounding the observation of PyC mineralisation over a small fraction of the expected MRT of PyC.

If all legacy sinks and sources are considered then a second, indirect set of variables for the fire C-balance condition can be formulated in addition to Eq. 1:

$$\boldsymbol{SOC^{+}_{PyC} + PyC^{+}_{LW} = VC^{-}_{\Delta FiReg} + VC^{-}_{Mort} + SOC^{-}_{hfloss} + SOC^{-}_{PyCExp} + E^{-}_{PyC}} \quad \textit{(2)}$$

Including $\overline{SOC_{PyCExp}}$ means that Eq. 2 gives the net flux of post-fire C with respect to the terrestrial biosphere, not with respect to the atmosphere because we do not consider aquatic fluxes (Supplementary Text S1). In order for the terrestrial fire C cycle to be in steady state over decadal to centennial scales, *both* equations (1) and (2), must hold.

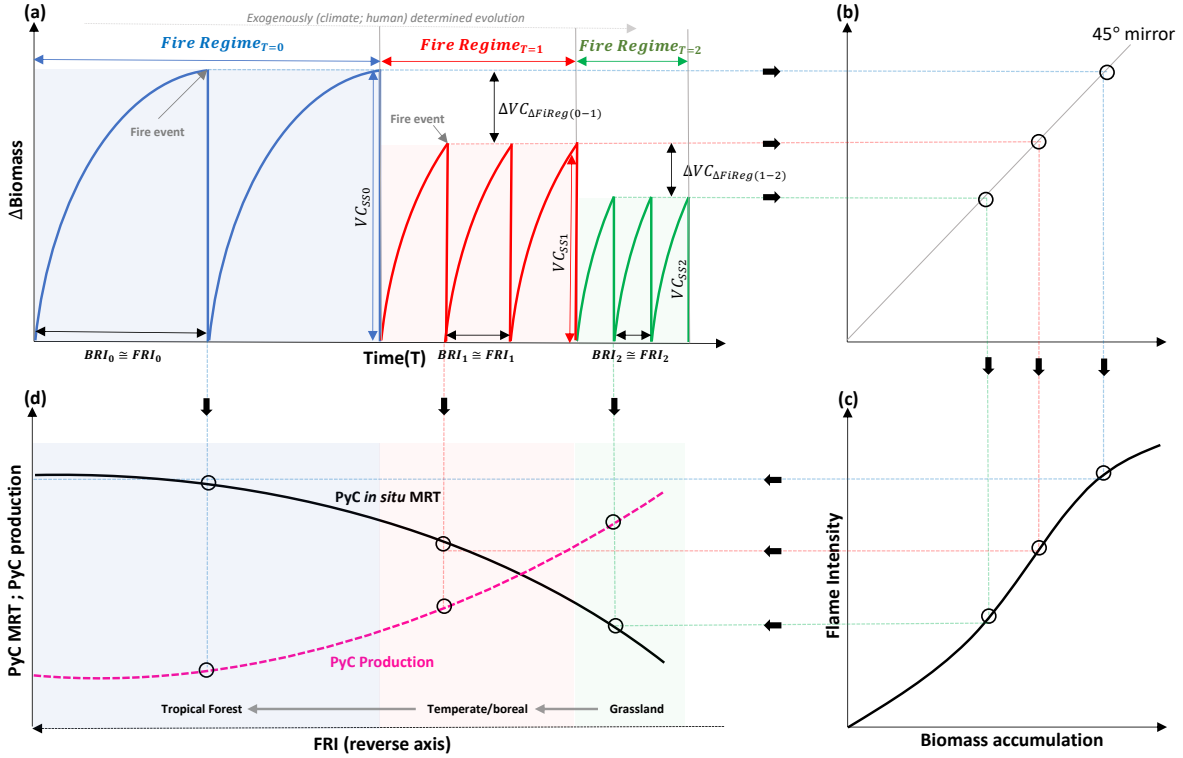

Figure 1: Schematic representation of the interrelation between plot or biome -scale: (a) Change of vegetation biomass post-fire to steady state (VC_{SSn}) and its evolution with change in fire regime ($FReg._n$), where subscript (n) refers to the specific fire regime as a f(time). Included is vegetative C-loss term due to change in FReg. *($\Delta VC_{\Delta FiReg(n-n+1)}$). (b) is a graphic aid to mirror the y-axis in (a) onto the x-axis in (c). (c) Fire intensity and terrestrial biomass accumulation (assumed here to be directly proportionate to ΔBiomass in (a)). (d) PyC production and its mean residence time with FRI (reverse axis) and flame intensity in (c). Sub-graphs (a,c,d) are thus related to one another by the coloured dashed lines. Refs.:* [2,4,5,11,18–21]

Mechanistic models of the terrestrial carbon cycle have thus far failed to include the legacy sinks and sources invoked by fire. Here we, integrate these fluxes into a dynamic global vegetation model (DGVM) to provide the first estimate of the annualised components of the legacy C cycle of fire represented by Eq. 2 (see *Methods*). Specifically, we incorporate dynamic PyC production by fires into ORCHIDEE-MICT (rev.8.9.1),[2223,24] and run the model globally (0.5° resolution, monthly timestep) over 1901-2010 forced by historical CO_2, imposed vegetation (ESA-LUH2) and CRU-NCEP v8[25] climatology (*Methods*). We investigate the spatio-temporal dynamics of the legacy fluxes over the 20th Century and quantify a fire C balance for global biomes (*Methods*, Fig. S1). C loss terms in Eq. 2 are derived offline from model output (*Methods*). FRI is determined for each grid cell and plant type as a probabilistic function of fire CO_2 emissions (*Methods*, *Fig. S2*). A hybrid model-data approach estimates the vegetation-specific BRI of each pixel(*Methods*). We do not explicitly estimate global mean PyC mineralisation ($\overline{E_{PyC}}$) but rather derive its maximum value from the residual of other terms that form Eq. 2.

20th Century Patterns of PyC Production

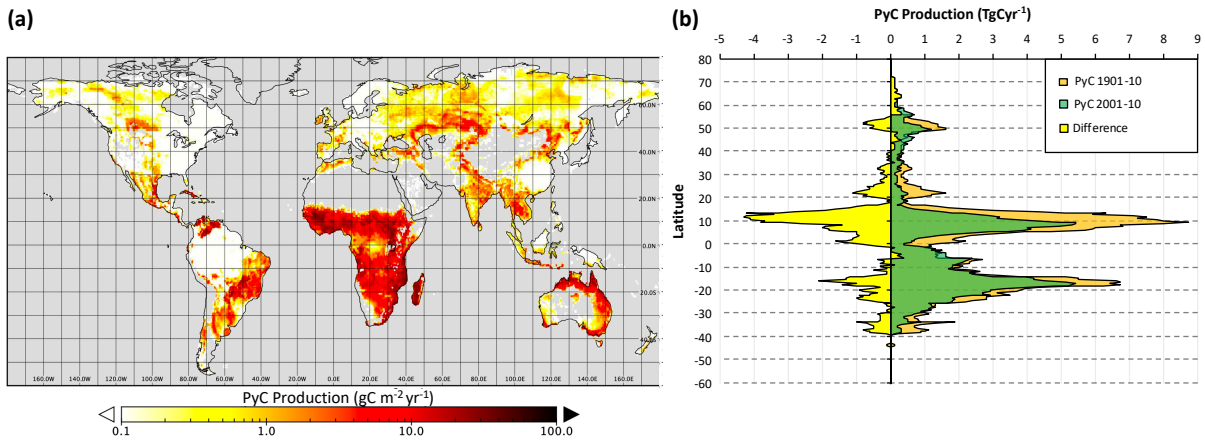

Figure 2: Simulated PyC production and change over 1901-2010. (a) Map of global PyC production averaged over the entire simulation period (log gC $m^{-2}yr^{-1}$). (b) Simulation-averaged annual absolute PyC production summed per 0.5° latitude bin (TgC yr^{-1}) in 1901-10 (orange) and 2001-10 (green), with the difference (latter-former) shown in yellow.

Over 1901-2010, we estimate average annual PyC production of 281 (188-424) TgC-PyC yr^{-1}, similar to a previous estimate for the period 1997-2016 based on a simpler estimate driven by satellite observations of fire (256 (196-340) TgC yr^{-1})[2]. Around 73-79% of PyC is produced in C4 and C3 (13-17%) grasslands (Fig. S3). Large interannual variations (251-345 TgC yr^{-1}) are symptomatic of trends over the 20thC[27–29], when PyC production declined from an average of 298 to 269 TgC yr^{-1} between the first and last 3 decades, largely reflecting climatic and anthropogenically-forced changes in fire phenomena (e.g. human suppression, *Methods*). Distribution of PyC is consistent with that of fires generally, with the bulk occurring in the range 20°N-30°S (Fig. 2a,b)[2]. However, declines in PyC production are marked by their divergence from this bulk latitudinal distribution, occurring almost entirely in the northern hemisphere, with some PyC production gains in the southern tropics (Fig. 2b), reflecting grassland degradation in the former and climatic changes (e.g. increasing aridity) in the latter (Figs. S5,S6,S8).

Globally, fires affect all biomes but do so in disproportion to their respective surface areas. Roughly 80% of global burning occurs in grassland-savannah dominated regions[30], despite these today only accounting for ~30-40% of the global land surface[31,3226]. This mismatch is caused by the evolutionary niche and adaptation of grasslands, enabling them to thrive where tree cover is limited by environmental conditions[33]. Grasses preferentially allocate biomass to belowground organs, allowing them to function immediately after, and rapidly recover from, disturbance [34,35]. Rapid post-disturbance vegetative and fuel stock recovery (BRI <1-3 yr[11,26]) lay the ground for the rapid return of fire events, since tropical grassland fires are typically dominantly fuel-limited[36], and fire returns almost as soon as vegetation has recovered (FRI≅BRI). This feature of tropical grasslands is important to Eq. 2, since whereas loss terms VC^{-}_{Mort} and $VC_{\Delta FiReg}$ are dependent on relative FRI:BRI, the gain term SOC^{+}_{PyC} is an absolute quantity, meaning simply that the more fire there is the more PyC is injected into the global soil mass (Fig.1). Due to high fire frequency and recovery rates, grassland biomes are both the main source of PyC globally (~250 TgCyr^{-1}), and, compared to other vegetation types, pull the relative sink and source terms of Eq. 2 towards the former.

In grasslands, simulation-average annual PyC production fell globally by 8% relative to the simulation mean pre- and post- 1930, when conversion to agriculture or plantation forest during the 'Dust Bowl' era resulted in a reduction in grassland cover in the Great Plains by up to -96%[26,37], with subsequent distributional changes in fire and PyC production (Fig. S4). The

years after 1930 saw the gradual rollout of conversions[38] of grassland to agriculture at global scale, resulting in average changes of -59 TgCyr^{-1} and +37 TgCyr^{-1} in grass and forest SOC^{+}_{PyC}, respectively. Our vegetation maps show -21% (-1.16 Mkm^2) and -12% (-3.6 Mkm^2) net declines in C3 and (tropical) C4 grasslands between the first and last decades of simulation (Fig. S5), leading to global, correlated decreases PyC production (Fig. 3i, Fig S6), in spite of global forest PyC production doubling over the same period (Fig. S3). This is consistent with a generalised shortening of fire return intervals over the 20thC (Fig. S7). Where grassland coverage did increase, this was largely secondary vegetation arising from primary forest degradation[39].

These negative and positive PyC dynamics are, respectively, policy and climate -driven (Figs. S6, S8): Where PyC production rises, an increase in atmospheric CO_2 feeds into NPP and fuel loading, while increasing temperatures affect fuel moisture, potentially increasing fire ignitions globally. Where it falls, the native grassland conversions to plantation in the Great Plains, Central Eurasia, India, Thailand, Brazil /Argentina and Australia are clearly visible in Fig. S5, consistent with previous findings of reductions in potential terrestrial biomass due to agriculture[40,41]. PyC gain/loss is modulated by human fire suppression, largely responsible for an apparent decrease in fires in recent decades[27], resulting in decreasing mean flame intensity and fire duration post-1940 (Fig. S9). The net effect of these dynamics has been to decrease the partial fire C sink by up to half over the 20th Century (Fig. S10).

Emerging Constraints on PyC Storage

We approximate the vegetation-specific potential in situ MRTs of PyC by considering mean and maximum flame temperatures for each vegetation type (Table S2; see Methods). Surprisingly, we find that Tropical (C4) grasslands and savannah regions host some of the highest maximal and mean flame intensities, which confers correspondingly high PyC MRTs (Fig. 1), in contrast with C3 grassland fires whose intensities are lower than most vegetation types. The data also indicate that fires tree-dominated vegetation types are generally more intense than in grasslands despite the absence of crown fire representation, which can release very large amounts of energy[11,42,43], in ORCHIDEE[24]. This implies that the grass-forest dichotomy for PyC MRT proposed here may only hold for temperate grasslands (Fig.1, Table S2, Text S6), with tropical grasslands producing not only the highest quantity and but also some of the most recalcitrant PyC. Note that MRT is a global average, aggregating the broad variation in spatial (lateral/vertical) residence time distributions globally, as per the literature.

We also derive the ceiling value of the PyC mineralisation flux (E^{-}_{PyC}) from the residual of other terms included in Eq. 2. Over 1901-2010, average global legacy carbon sinks through PyC production (SOC^{+}_{PyC}; 281 (188-424) TgC yr^{-1}) and lightweight PyC input (PyC^{+}_{LW} = 56 (45-90) TgC yr^{-1}) are partially countered by legacy sources from vegetative non-recovery ($VC_{\Delta FiReg}$ = 46 (27-53), Fig. S11), high frequency fire topsoil degradation (SOC^{-}_{hfloss} = 57 (30-95) TgC yr^{-1}, Fig. S12), PyC aquatic export (SOC^{-}_{PyCExp} = 44(28-59) TgC yr^{-1}, Fig. S13), and annualised tropical drought-induced fire mortality (VC^{-}_{Mort} = 24 (21-28) TgC yr^{-1}, Fig. S14). Excluding E^{-}_{PyC}, the legacy fluxes are imbalanced and indicate a partial terrestrial C sink of 177 TgC yr^{-1} (Fig. 3). We propose that the net partial balance of 177 TgC yr^{-1} provides an upper constraint on the annual mineralisation of PyC to the atmosphere (E^{-}_{PyC}). This value falls in the middle of the (E^{-}_{PyC}) range observation-based estimates in previous work[4]. Note that combustion of PyC in subsequent 'reburn' events[44] are considered a component of E^{-}_{PyC} here.

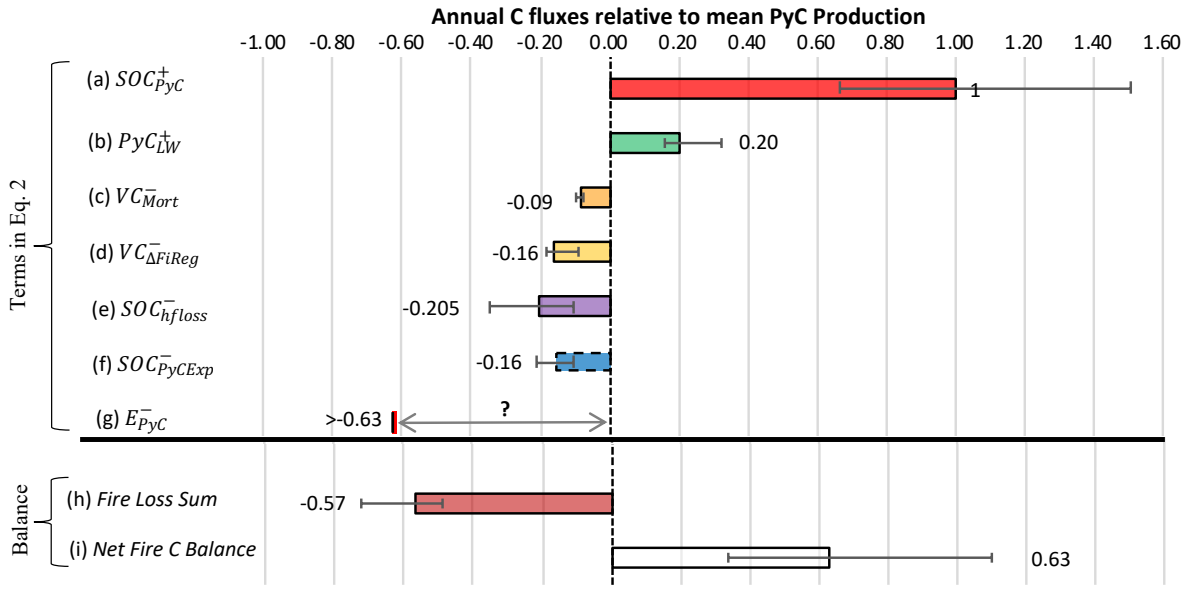

Figure 3: Time averaged estimates for the source and sink terms in Eq. 2 (top), with the PyC mineralisation loss quantity unknown, but constrained by the net fire C balance. SOC^{-}_{PyCExp} is dotted to highlight that it is a terrestrial export flux, not an atmospheric flux. Bottom panel shows aggregations of (h) fire C losses (sum of (c→f)) and (i) the fire C balance net of PyC mineralisation, i.e. the sum of (a→b) and (c→f). Maximum mineralisation (g) is thus equal to the residual, (i).

Regional Distribution of Fire-induced C Sinks and Sources

While absolute fire C gains and losses are highest in the tropics (Fig. 4a), the highest ratio of gains to losses (efficiency of the fire C sink) lies in the temperate north (30-60N), with a factor of ~3, and lowest (factor 1.6) in the tropical south (0-30S). The positive partial balance is strongest in the south, consistent with the quantity of PyC production, with some negative balance areas occurring as a result of combined FRI decrease and topsoil loss (Figs. 4c, S4-S7). However, the partial balance over all vegetation types masks the fact that when considering grasslands and forests separately, the latter on aggregate exhibit strongly negative partial balance estimates, with the greatest negative factorials in the southern hemisphere at 0-30 and 30-60S (factors of -3 and -8, respectively, Fig. 4b), providing powerful suggestive evidence that grasses and forest play contrasting functional roles with respect to fire in the terrestrial C balance.

Overall, over the period of our simulation, our results indicate that when aggregated over space and vegetation types, fires may provide a long-term C sink made possible by the buffers of PyC production[2] and biospheric uptake, provided that the fire regime remains in state that does not lead to ecosystem degradation from failed recovery (FRI≥BRI). By way of simple back-envelope calculation, our ceiling PyC mineralisation (177 $TgCyr^{-1}$) sits well within the range of a prior PyC in situ (terrestrial and freshwater) MRT estimate of 3700 yrs[7], 1st-order PyC stock estimates (14% global SOC)[18] and bulk SOC mineralisation of ~70 $PgCyr^{-1}$)[45,46]. PyC mineralisation of 177 TgC yr^{-1} is at least 55 times that non-PyC bulk SOC, which assuming global SOC MRT of ~50 yrs[6] gives minimum PyC MRT of ~2760 yrs (SI Text S7). This mean value, which is higher than many laboratory-based incubations studies[47], may further validate findings showing broad PyC storage in terrestrial 'holding areas' for thousands of years[7].

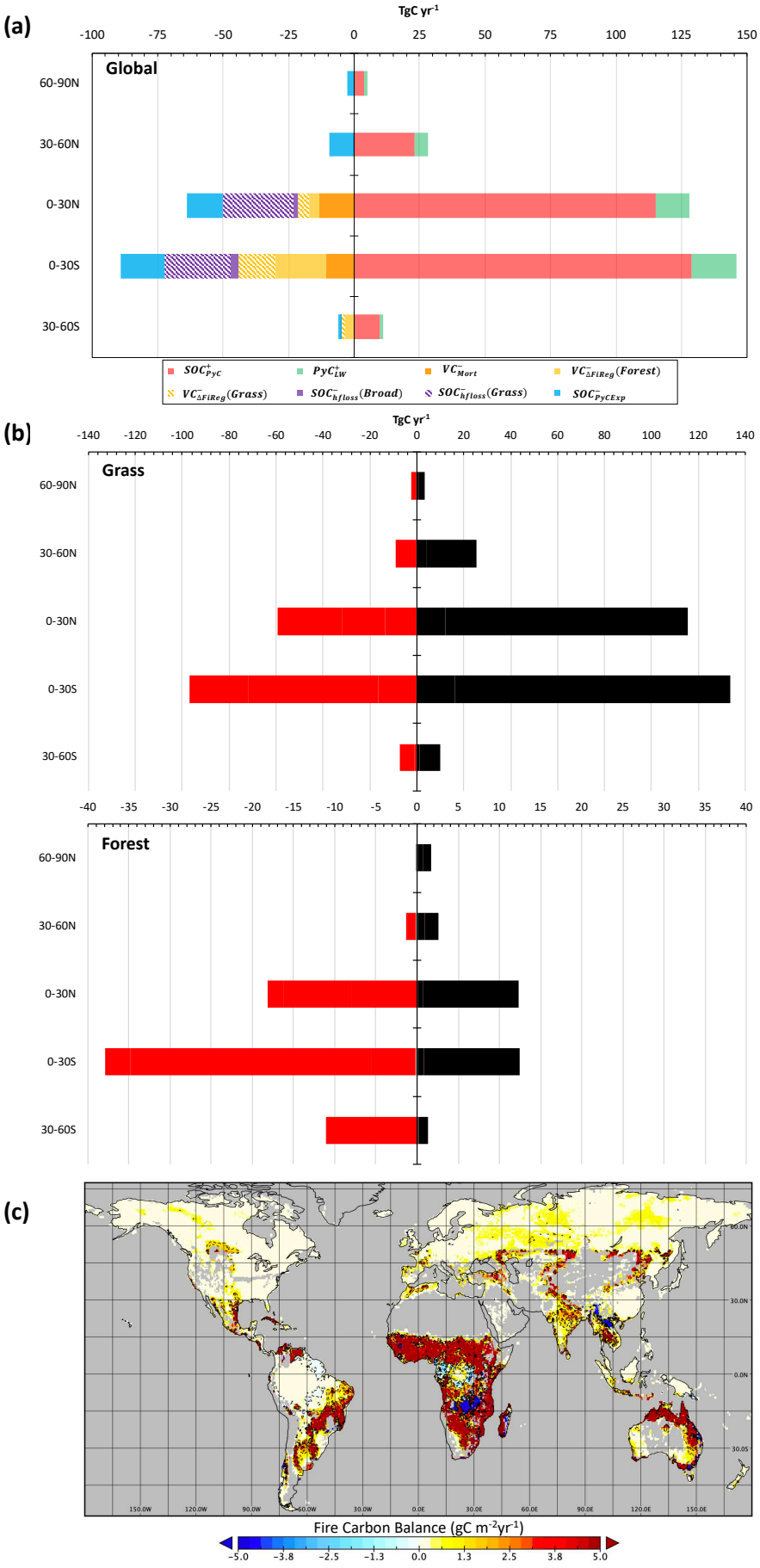
(a)
TgC yr-1
-100 -75 -50 -25 0 25 50 75 100 125 150
Global
60-90N
30-60N
0-30N
0-30S
30-60S
SOC^{+}_{PyC}
PyC^{+}_{LW}
VC^{-}_{Mort}
$VC^{-}_{\Delta FiReg}(Forest)$
$VC^{-}_{\Delta FiReg}(Grass)$
$SOC^{-}_{hfloss}(Broad)$
$SOC^{-}_{hfloss}(Grass)$
SOC^{-}_{PyCExp}
(b)
TgC yr-1
-140 -120 -100 -80 -60 -40 -20 0 20 40 60 80 100 120 140
Grass
60-90N
30-60N
0-30N
0-30S
30-60S
-40 -35 -30 -25 -20 -15 -10 -5 0 5 10 15 20 25 30 35 40
Forest
60-90N
30-60N
0-30N
0-30S
30-60S
(c)
Fire Carbon Balance (gC m-2yr-1)
-5.0 -3.8 -2.5 -1.3 0.0 1.3 2.5 3.8 5.0

247

Figure 4: (a) Time-averaged (1901-2010) sources and sinks in the global fire C-cycle, summed per 30-degree latitudinal band, in TgC yr^{-1}. Note that fire regime change and high frequency fire SOC loss terms are disaggregated between forest (solid) and grass (dashed), and that the colour legend for each term is equivalent to that in Figure 3. (b) Comparison of time-averaged grassland (left) and forest (right) fire C sources (red) and sinks (black) summed per 30° bin (as in (a)), in TgC yr^{-1}. (c) Global map of the time-averaged fire-C 'balance' (gC m^{-2} yr^{-1}) for each pixel, with iso-lines included, where negative values indicate C-source, and positive a C-sink. The balance is calculated as the net sum of Eq. 2, excluding the PyC mineralisation term (E_{PyC}^{-}), which is unknown.

Re-thinking the Role of Fire in the Carbon Cycle

Our work indicates that net of legacy fluxes fires in may be a force for Earth System C equilibrium, provided that they ignite over biomes (e.g. grasslands) that carry evolutionary adaptations to cope with them. This is somewhat counterintuitive given the dramatic nature of wildfires and their large initial emissions, which feed a perception of destabilisation[48]. Forest fire-induced C losses are compensated globally by the dynamics of grassland ignition, despite considerable post-fire grassland SOC losses (~52vs.5 TgC yr^{-1} for grass, forest respectively).

We estimate that fire regime change-induced C loss ($VC_{\Delta FiReg}$) in grasslands is less than that associated with forests (~20 vs 26 TgC yr^{-1}). This result is afforded by grasses' capacity for fire recovery[49–53], providing large stocks of aboveground fuel (potential PyC), thereby mitigating losses and maximising soil PyC gains. Thus, PyC production is less correlated to flame intensity/temperature for grassland than forests (Fig. S15). In the absence of grasslands, fire phenomena would impose a net terrestrial C source. This aligns with the proposition that the co-evolution of grassland fire and herbivory led to the formation of PyC-rich Mollisols that may have been central to climatic cooling since the Mid-Cenozoic (~40-0Ma)[35]. Conversely, the fire-as-destabilisation perspective *is* justified in biome-specific cases, generalisable to non-grass (forest) fires (Fig. 4b).

In forests, fire C losses can overwhelm PyC gains even without considering PyC mineralisation. This is not surprising, particularly in the humid tropics, where tree species are ill-adapted to catastrophic disturbance[54,55] and massive post-fire mortality is commonplace[12–14,54](Fig. S14). Similarly, subtropical and semi-arid regions may be more prone to fire events of higher intensity[11], resulting in topsoil loss and an incapacity for biomass recovery, in addition to aquatic outflows of C (Fig 4a, S13).

The dependency of the partial fire C balance on fire-affected vegetation composition has important implications for a world in which the frequency and intensity of droughts, heatwaves and wind extremes[56–64], are forecast to increase[65–70], potentially increasing all terms in Eq.2. The preservation and restoration of native grasslands may be seen as an important vector for increasing C stocks/decreasing C losses from future fire activity, and would apply to both temperate and tropical systems, given the efficiency of the former as a C-sink (Fig.4b) and the contribution of the latter to PyC production (Fig. S3) and bulk PyC MRT (Table S2). Tropical grasslands have until recently been ignored in the landscape restoration narrative[26,33,34,39,71] and are rarely discussed in 'carbon farming' initiatives[72], although this is now changing[73,74]. Greater understanding of fire legacy C fluxes and the effects of human deforestation on these will enable clearer diagnosis of the state and future direction of the full global fire C balance and attendant land management decisions.

References

1. Van Marle, M. J. E. *et al.* Historic global biomass burning emissions for CMIP6 (BB4CMIP) based on merging satellite observations with proxies and fire models (1750-2015). *Geoscientific Model Development* (2017). doi:10.5194/gmd-10-3329-2017
2. Jones, M. W., Santín, C., van der Werf, G. R. & Doerr, S. H. Global fire emissions buffered by the production of pyrogenic carbon. *Nat. Geosci.* (2019). doi:10.1038/s41561-019-0403-x
3. Santín, C. *et al.* Towards a global assessment of pyrogenic carbon from vegetation fires. *Global Change Biology* (2016). doi:10.1111/gcb.12985
4. Bird, M. I., Wynn, J. G., Saiz, G., Wurster, C. M. & McBeath, A. The pyrogenic carbon cycle. *Annu. Rev. Earth Planet. Sci.* (2015). doi:10.1146/annurev-earth-060614-105038
5. Hammes, K. & Abiven, S. Identification of Black Carbon in the Earth System. in *Fire Phenomena and the Earth System: An Interdisciplinary Guide to Fire Science* (2013). doi:10.1002/9781118529539.ch9
6. Schmidt, M. W. I. *et al.* Persistence of soil organic matter as an ecosystem property. *Nature* (2011). doi:10.1038/nature10386
7. Coppola, A. I. *et al.* Global-scale evidence for the refractory nature of riverine black carbon. *Nat. Geosci.* (2018). doi:10.1038/s41561-018-0159-8
8. Kuzyakov, Y., Bogomolova, I. & Glaser, B. Biochar stability in soil: Decomposition during eight years and transformation as assessed by compound-specific 14C analysis. *Soil Biol. Biochem.* (2014). doi:10.1016/j.soilbio.2013.12.021
9. Singh, B. P., Cowie, A. L. & Smernik, R. J. Biochar carbon stability in a clayey soil as a function of feedstock and pyrolysis temperature. *Environ. Sci. Technol.* (2012). doi:10.1021/es302545b
10. Masiello, C. A. & Druffel, E. R. M. Black carbon in deep-sea sediments. *Science (80-.).* (1998). doi:10.1126/science.280.5371.1911
11. Archibald, S., Lehmann, C. E. R., Gómez-Dans, J. L. & Bradstock, R. A. Defining pyromes and global syndromes of fire regimes. *Proc. Natl. Acad. Sci. U. S. A.* (2013). doi:10.1073/pnas.1211466110
12. Brando, P. M. *et al.* Prolonged tropical forest degradation due to compounding disturbances: Implications for CO2 and H2O fluxes. *Glob. Chang. Biol.* (2019). doi:10.1111/gcb.14659
13. Silva, C. V. J. *et al.* Drought-induced Amazonian wildfires instigate a decadal-scale disruption of forest carbon dynamics. *Philos. Trans. R. Soc. B Biol. Sci.* (2018). doi:10.1098/rstb.2018.0043
14. Withey, K. *et al.* Quantifying immediate carbon emissions from El Niño-mediated wildfires in humid tropical forests. *Philos. Trans. R. Soc. B Biol. Sci.* (2018). doi:10.1098/rstb.2017.0312
15. Pellegrini, A. F. A. *et al.* Fire frequency drives decadal changes in soil carbon and nitrogen and ecosystem productivity. *Nature* (2018). doi:10.1038/nature24668
16. Jones, M. W. *et al.* Fires prime terrestrial organic carbon for riverine export to the global oceans. *Nat. Commun.* (2020). doi:10.1038/s41467-020-16576-z
17. Qi, Y. *et al.* Dissolved black carbon is not likely a significant refractory organic carbon pool in rivers and oceans. *Nat. Commun.* (2020). doi:10.1038/s41467-020-18808-8
18. Reisser, M., Purves, R. S., Schmidt, M. W. I. & Abiven, S. Pyrogenic carbon in soils: A literature-based inventory and a global estimation of its content in soil organic carbon and stocks. *Front. Earth Sci.* (2016). doi:10.3389/feart.2016.00080

19. Schmidt, H. P. *et al.* Pyrogenic carbon capture and storage. *GCB Bioenergy* (2019). doi:10.1111/gcbb.12553
20. Abiven, S. & Santín, C. Editorial: From fires to oceans: Dynamics of fire-derived organic matter in terrestrial and aquatic ecosystems. *Frontiers in Earth Science* (2019). doi:10.3389/feart.2019.00031
21. Fu, Z. *et al.* Recovery time and state change of terrestrial carbon cycle after disturbance. *Environ. Res. Lett.* (2017). doi:10.1088/1748-9326/aa8a5c
22. Guimberteau, M. *et al.* ORCHIDEE-MICT (v8.4.1), a land surface model for the high latitudes: model description and validation. *Geosci. Model Dev.* **11**, 121–163 (2018).
23. Thonicke, K. *et al.* The influence of vegetation, fire spread and fire behaviour on biomass burning and trace gas emissions: Results from a process-based model. *Biogeosciences* (2010). doi:10.5194/bg-7-1991-2010
24. Yue, C. *et al.* Modelling the role of fires in the terrestrial carbon balance by incorporating SPITFIRE into the global vegetation model ORCHIDEE - Part 1: Simulating historical global burned area and fire regimes. *Geosci. Model Dev.* (2014). doi:10.5194/gmd-7-2747-2014
25. Viovy, N. CRUNCEP Version 7 - Atmospheric Forcing Data for the Community Land Model. *Research Data Archive at the National Center for Atmospheric Research, Computational and Information Systems Laboratory* (2018). doi:https://doi.org/10.5065/PZ8F-F017. Accessed 22/02/2020
26. Leys, B. A., Marlon, J. R., Umbanhowar, C. & Vannière, B. Global fire history of grassland biomes. *Ecol. Evol.* (2018). doi:10.1002/ece3.4394
27. Andela, N. *et al.* A human-driven decline in global burned area. *Science (80-.).* (2017). doi:10.1126/science.aal4108
28. Arora, V. K. & Melton, J. R. Reduction in global area burned and wildfire emissions since 1930s enhances carbon uptake by land. *Nat. Commun.* (2018). doi:10.1038/s41467-018-03838-0
29. Forkel, M. *et al.* Recent global and regional trends in burned area and their compensating environmental controls. *Environ. Res. Commun.* (2019). doi:10.1088/2515-7620/ab25d2
30. Mouillot, F. & Field, C. B. Fire history and the global carbon budget: A 1° × 1° fire history reconstruction for the 20th century. *Global Change Biology* (2005). doi:10.1111/j.1365-2486.2005.00920.x
31. Gibson, D. *Grasses & grassland ecology*. *Annals of Botany* (2009).
32. Dixon, A. P., Faber-Langendoen, D., Josse, C., Morrison, J. & Loucks, C. J. Distribution mapping of world grassland types. *J. Biogeogr.* (2014). doi:10.1111/jbi.12381
33. Buisson, E. *et al.* Resilience and restoration of tropical and subtropical grasslands, savannas, and grassy woodlands. *Biol. Rev.* (2019). doi:10.1111/brv.12470
34. Bond, W. J. Ancient grasslands at risk. *Science* (2016). doi:10.1126/science.aad5132
35. Retallack, G. J. Global cooling by grassland soils of the geological past and near future. *Annu. Rev. Earth Planet. Sci.* (2013). doi:10.1146/annurev-earth-050212-124001
36. Alvarado, S. T., Andela, N., Silva, T. S. F. & Archibald, S. Thresholds of fire response to moisture and fuel load differ between tropical savannas and grasslands across continents. *Glob. Ecol. Biogeogr.* (2020). doi:10.1111/geb.13034
37. White, R., Murray, S. & Rohweder, M. *Pilot Analysis of Global Ecosystems: Grassland Ecosystems. World Resources Institute* (2000). doi:10.1021/es0032881
38. Visser, J. *Down to earth: a historical-sociological analysis of the rise and fall of 'industrial' agriculture and of the prospects for the re-rooting of agriculture from the*

factory to the local farmer and ecology. (Wageningen University, 2010).
39. Silveira, F. A. O. *et al.* Myth-busting tropical grassy biome restoration. *Restor. Ecol.* (2020). doi:10.1111/rec.13202
40. Erb, K. H. *et al.* Unexpectedly large impact of forest management and grazing on global vegetation biomass. *Nature* (2018). doi:10.1038/nature25138
41. Haberl, H., Erb, K. H. & Krausmann, F. Human appropriation of net primary production: Patterns, trends, and planetary boundaries. *Annual Review of Environment and Resources* (2014). doi:10.1146/annurev-environ-121912-094620
42. Rogers, B. M., Soja, A. J., Goulden, M. L. & Randerson, J. T. Influence of tree species on continental differences in boreal fires and climate feedbacks. *Nat. Geosci.* (2015). doi:10.1038/ngeo2352
43. De Groot, W. J. *et al.* A comparison of Canadian and Russian boreal forest fire regimes. *For. Ecol. Manage.* (2013). doi:10.1016/j.foreco.2012.07.033
44. Doerr, S. H., Santín, C., Merino, A., Belcher, C. M. & Baxter, G. Fire as a Removal Mechanism of Pyrogenic Carbon From the Environment: Effects of Fire and Pyrogenic Carbon Characteristics. *Front. Earth Sci.* (2018). doi:10.3389/feart.2018.00127
45. Huang, N. *et al.* Spatial and temporal variations in global soil respiration and their relationships with climate and land cover. *Sci. Adv.* **6**, eabb8508 (2020).
46. Warner, D. L., Bond-Lamberty, B., Jian, J., Stell, E. & Vargas, R. Spatial Predictions and Associated Uncertainty of Annual Soil Respiration at the Global Scale. *Global Biogeochem. Cycles* (2019). doi:10.1029/2019GB006264
47. Singh, N., Abiven, S., Torn, M. S. & Schmidt, M. W. I. Fire-derived organic carbon in soil turns over on a centennial scale. *Biogeosciences* (2012). doi:10.5194/bg-9-2847-2012
48. Stenzel, J. E. *et al.* Fixing a snag in carbon emissions estimates from wildfires. *Glob. Chang. Biol.* (2019). doi:10.1111/gcb.14716
49. Coutinho, L. M. Fire in the Ecology of the Brazilian Cerrado. in (1990). doi:10.1007/978-3-642-75395-4_6
50. Appezzato-da-Glória, B., Cury, G., Soares, M. K. M., Rocha, R. & Hayashi, A. H. Underground systems of Asteraceae species from the Brazilian Cerrado. *J. Torrey Bot. Soc.* (2008). doi:10.3159/07-RA-043.1
51. Fidelis, A. & Blanco, C. Does fire induce flowering in Brazilian subtropical grasslands? *Appl. Veg. Sci.* (2014). doi:10.1111/avsc.12098
52. Veldman, J. W. *et al.* Toward an old-growth concept for grasslands, savannas, and woodlands. *Frontiers in Ecology and the Environment* (2015). doi:10.1890/140270
53. Simon, M. F. *et al.* Recent assembly of the Cerrado, a neotropical plant diversity hotspot, by in situ evolution of adaptations to fire. *Proc. Natl. Acad. Sci. U. S. A.* (2009). doi:10.1073/pnas.0903410106
54. Brando, P. M. *et al.* Droughts, Wildfires, and Forest Carbon Cycling: A Pantropical Synthesis. *Annual Review of Earth and Planetary Sciences* (2019). doi:10.1146/annurev-earth-082517-010235
55. Chambers, J. Q., Higuchi, N. & Schimel, J. P. Ancient trees in Amazonia [10]. *Nature* (1998). doi:10.1038/34325
56. Trenberth, K. E. Changes in precipitation with climate change. *Clim. Res.* (2011). doi:10.3354/cr00953
57. Donat, M. G., Lowry, A. L., Alexander, L. V., O'Gorman, P. A. & Maher, N. More extreme precipitation in the worldâ €TM s dry and wet regions. *Nat. Clim. Chang.* (2016). doi:10.1038/nclimate2941
58. Prein, A. F. *et al.* The future intensification of hourly precipitation extremes. *Nat. Clim. Chang.* (2017). doi:10.1038/nclimate3168

59. Wu, P., Christidis, N. & Stott, P. Anthropogenic impact on Earth's hydrological cycle. *Nat. Clim. Chang.* (2013). doi:10.1038/nclimate1932
60. Kunkel, K. E. *et al.* Probable maximum precipitation and climate change. *Geophys. Res. Lett.* (2013). doi:10.1002/grl.50334
61. Yin, J. *et al.* Large increase in global storm runoff extremes driven by climate and anthropogenic changes. *Nat. Commun.* (2018). doi:10.1038/s41467-018-06765-2
62. Walsh, K. J. E. *et al.* Tropical cyclones and climate change. *Wiley Interdiscip. Rev. Clim. Chang.* (2016). doi:10.1002/wcc.371
63. Abatzoglou, J. T., Williams, A. P. & Barbero, R. Global Emergence of Anthropogenic Climate Change in Fire Weather Indices. *Geophys. Res. Lett.* (2019). doi:10.1029/2018GL080959
64. Jia, G. *et al.* Land–climate interactions. in *Climate Change and Land: an IPCC special report on climate change, desertification, land degradation, sustainable land management, food security, and greenhouse gas fluxes in terrestrial ecosystems.* (2019).
65. Barbero, R., Abatzoglou, J. T., Larkin, N. K., Kolden, C. A. & Stocks, B. Climate change presents increased potential for very large fires in the contiguous United States. *Int. J. Wildl. Fire* (2015). doi:10.1071/WF15083
66. Stephens, S. L. *et al.* Managing forests and fire in changing climates. *Science* (2013). doi:10.1126/science.1240294
67. Moritz, M. A. *et al.* Climate change and disruptions to global fire activity. *Ecosphere* (2012). doi:10.1890/es11-00345.1
68. Flannigan, M. *et al.* Global wildland fire season severity in the 21st century. *For. Ecol. Manage.* (2013). doi:10.1016/j.foreco.2012.10.022
69. Knorr, W., Arneth, A. & Jiang, L. Demographic controls of future global fire risk. *Nat. Clim. Chang.* **6**, 781–785 (2016).
70. Pechony, O. & Shindell, D. T. Driving forces of global wildfires over the past millennium and the forthcoming century. *Proc. Natl. Acad. Sci. U. S. A.* (2010). doi:10.1073/pnas.1003669107
71. Nerlekar, A. N. & Veldman, J. W. High plant diversity and slow assembly of old-growth grasslands. *Proc. Natl. Acad. Sci. U. S. A.* (2020). doi:10.1073/pnas.1922266117
72. Bastin, J. F. *et al.* The global tree restoration potential. *Science (80-.).* (2019). doi:10.1126/science.aax0848
73. Hungate, B. A. *et al.* The economic value of grassland species for carbon storage. *Sci. Adv.* (2017). doi:10.1126/sciadv.1601880
74. Strassburg, B. B. N. *et al.* Global priority areas for ecosystem restoration. *Nature* (2020). doi:10.1038/s41586-020-2784-9

Author contributions

S.P.K.B. and S.Z designed the study. S.P.K.B. performed the code implementation in ORCHIDEE, set up the simulations and processed the output used for this study. M.W.J. provided access to data and insight to the PyC production factors used in the simulations. P.C. and B.G. provided additional input to the coding and data processing processes. All authors contributed to the interpretation of the results. S.P.K.B. wrote the manuscript and produced all figures, M.W.J. made substantial additions to the text. All authors contributed to final modifications of the manuscript.

Competing interests

The authors declare no competing interests.

Methods

Model description:

Here we apply PyC production to the IPSL Earth System Model, ORCHIDEE-MICT revision number 5308, a widely used sub-branch of ORCHIDEE that is global in scope but includes some soil, hydrological and thermal processes specific to boreal regions [1–3] , whose use here will facilitate future assessments of PyC stocks in deep permafrost soils. At the core of the model is terrestrial biomass fixed by photosynthetic C uptake, performed by 13 plant functional types (PFTs) with distinct primary production, senescence and carbon dynamics[4]. Biomass is allocated to foliage, fruit, roots, above/below -ground sap, heart wood and carbon reserves which are transfered to two reactivity-differentiated litter pools. ORCHIDEE-MICT is integrated with a model-specific version (see ([5,6]))of the SPITFIRE fire module[5,7,8], which takes the aboveground portion of these biomass components and allocates them to potential fire fuel classes differentiated by their potential time to combustion/oxidation. ORCHIDEE-SPITFIRE has been involved in multiple phases of FireMIP[9] and its predictions found to be within the range of those from available fire models[10–13]. Fire ignitions are controlled by lightning strikes and human ignitions, the latter of which is determined as a positive logistic function of population density. Vegetation flammability is determined by fuel and climatic conditions (Nesterov Index and Fire Danger Index). Burned area is controlled by fire spread rate and fire duration, as influenced by vegetation flammability, and affects fire CO_2 emissions.

Modelled PyC Production:

PyC is produced in ORCHIDEE-MICT as a function of fuel class-specific fire CO_2 emissions using an adaptation of the apportioning between PyC production and fire CO_2 emissions estimate by Jones et al. (2019)[14], which posits central literature-based prediction of ratios $[SOC_{PyC}: E_{CO2}]$ of 0.261, 0.1 and 0.091 gPyC produced g^{-1} CO_2-C emitted, for the three fuel classes of Coarse Woody Fuels (CWF), Fine Woody Fuels (FWF), and Non Woody Fuels (NWF), respectively. Uncertainty in PyC production (Fig. 3) is based on the bootstrapped 95% confidence interval range in Jones et al. (2019), for PyC production ratios ($[SOC_{PyC}: E_{CO2}]$, gPyC-C g^{-1} CO_2-C) for CWF(0.176-0.389), FWF(0.064-0.153) and NWF(0.074-0.114) and applying the fractional difference of each bound from the central bound to PyC produced in the post-processing analysis. We apportion these to the four SPITFIRE fuel classes such that (1hr fuels→NWF), (10hr; 100hr fuels → FWF), (1000hr fuels → CWF), where the hour-term in SPITFIRE fuel classes refers to the order of magnitude of time required for the fuel to lose 63% of its moisture under idealized atmospheric conditions[8], determined effectively by the stem thickness of each biomass component of each PFT based on the 'average individual' of each woody PFT.

C mass balance is maintained by removing PyC produced from other C pools. PyC produced is first subtracted from the fraction of biomass going to litter pools in that SPITFIRE timestep (1 day). If PyC produced > biomass going to litter in that timestep, then the remaining quantity is taken from CO_2 emissions, whose reduction recursively reduces total PyC production. PyC is then introduced to the biosphere-pedosphere interface by its allocation to PyC-specific SOC reactivity pools, complementing the traditional CENTURY 3-pool model[15], with a 'Slow PyC' pool composed of (PyC_{10hr} + PyC_{100hr}), and a 'Passive PyC' pool (PyC_{1000hr}), where the subscript refers to the source fuel class of PyC. In the present configuration, PyC_{1hr} does not enter into either of the SOC pools and once produced, is instead added to the pool of dead biomass that becomes litter, which is then subject to normal model SOC dynamics (SI Text S2).

Once produced, the PyC SOC pools are immediately redistributed equally amongst the top 2.1cm of the model's vertically discretized soil layers to represent the initial translocation of PyC in the first year of production, following field observations from ref. ([16]). PyC pools are not exchanged with one another or with the other SOC pools, and are subjected to vertical bio- and cryo- turbation processes in the soil, and temperature and moisture - dependent mineralization Mineralisation rates are equivalent to bulk MRTs of ~300 and ~3000yrs for Slow and Passive PyC, respectively.

Simulation Configuration:

The simulations used for this study were forced with imposed historical 13-PFT vegetation (ESA-LUH2 v1.2), CRU-NCEP v8[17] climatology and atmospheric CO_2 concentrations at 0.5° resolution with SPITFIRE activated and hydrological river routing deactivated. Deforestation fires were deactivated and agricultural fires in the output ignored to simplify analysis. A 50 year 'spinup' run on a loop of the years 1901-1920 for the above input forcing datasets was first performed to bring the biosphere and fire cycle to a quasi-steady state under the closest pre-20th Century climatology we can approximate with our climate data. The same model was then run continuously over years 1901-2010. Fire C loss terms were estimated from derived variables in the simulation output.

Estimating PFT-specific Fire Return Interval (FRI):

PFT-specific FRI is defined as the interval between consecutive fires affecting a consistent area, which is not a standard output of ORCHIDEE and so was determined probabilistically. To do so, first we find the annual fractional fire contribution of each PFT ($fFire_{PFT}$) to total CO2 emissions:

$$\boldsymbol{fFire_{PFT} = EFire_{PFT} / \Sigma(EFire_{PFT})} \quad \textbf{(3)}$$

From this the probabilistic fire incidence per PFT, pixel and year can be estimated:

$$\boldsymbol{p(Fire)_{PFT} = fPFT_{Pix} * fFire_{PFT} * BA_{Pix}} \quad \textbf{(4)}$$

Where $p(Fire)_{PFT}$ is the annual probabilistic fire incidence per PFT and pixel, and $fPFT_{Pix}$ the fraction of each PFT occupied by vegetation from a given PFT ($\boldsymbol{fPFT_{Pix}}$). Global probabilistic FRI (yrs) for each pixel and PFT (FRI_{PFT}) over a given unspecifiable surface area (e.g. one hectare) can then be calculated by dividing $p(Fire)_{PFT}$ by PFT-specific vegetated area, giving the probability that a given hectare occupied by a given PFT in that pixel is the one that burned that year. This is summed over the simulation years then divided over the simulation length (110yrs). 1/ this value gives the FRI:

$$\boldsymbol{FRI_{PFT} = 1/((\sum_{t=1}^{110}(p(Fire)_{PFT}/(fPFT_{Pix} * Area_{Pix})))/110)} \quad \textbf{(5)}$$

The resulting gridded PFT specific map is then adapted to remove pixels where FRI > 1000 yrs, since this would largely result from insufficient sample size in time to adequately estimate the probabilistic FRI for these pixels/PFTs and adversely affect FRI-averaging calculations.

Estimating PFT-specific Biomass Recovery Interval (BRI):

Biomass carbon recovery times (the time for which a given surface area recovers all of the biomass lost due to a disturbance event) are difficult to quantify, and to our knowledge and no global gridded product estimating disturbance and PFT-specific biomass recovery times exists. We opted for a crude literature-based central value method to approximate PFT-specific BRI, modulated in space and time by the NPP of a pixel-specific PFT relative to the global median NPP of that PFT. We treated (a) C3 and C4 grasses, (b) all extra-tropical forest types, and (c) tropical forests, as separate categories. For (a) and (b), we assumed that for a given pixel and year, C losses from fire can be recovered by the completion of that time interval which itself varies by ±β as a function of the NPP experienced by that pixel relative to the global median NPP for that PFT:

$$\boldsymbol{BRI_{Pix}^{PFT} = BRI^{PFT} \pm (BRI^{PFT} * (\beta * NPP_{Pix}^{PFT} / \overline{NPPm_{Global}^{PFT}}))} \quad \textbf{(6)}$$

Where BRI_{Pix}^{PFT} is BRI per PFT, pixel and year, BRI^{PFT} is the central, global value of BRI, β is the fractional maximum variation of BRI_{Pix}^{PFT} from the central value, NPP_{Pix}^{PFT} the annual NPP of that PFT in a specific pixel and $\overline{NPPm_{Global}^{PFT}}$ is the time averaged global median NPP of that PFT. For C3 and C4 grasses, we set BRI^{PFT} at 2.5 and 1.5 years respectively, and β at ±25%, based on literature-based estimates and the assumption that tropical grasses have high NPP and recovery rates. For forests we set central BRI^{PFT} for all non-tropical forest PFTs to the value reported in a literature review -based study (fig. 4d of ref. [18]) of 133 years, which we then allow to vary (β) by ±50% as a function of NPP relative to $\overline{NPPm_{Global}^{PFT}}$ for each PFT. See the supplementary material for further discussion of parameter choices.

Estimating loss terms in Equation 2

Loss of biospheric C due to fire regime change ($\boldsymbol{VC_{\Delta FiReg}}$)

This loss term is calculated for each PFT and includes net C losses from areas where the biospheric disturbance steady state condition is not satisfied (BRI<FRI) as a result of a change in fire regime. We treat areas that experienced decreases in FRI of >10% between the first and last three decades of the simulation (Fig. S7), as having exhibited a fire regime shift. Then, we estimate the system biomass loss per fire event for these areas as the BRI:FRI ratio in the year of the event multiplied by the total CO_2 emissions from a given PFT in that year's fires:

$$\boldsymbol{VC_{\Delta FiReg} = (^{BRI_{PFT}}/_{FRI_{PFT}}) * E_{FCO2}} \quad \textbf{(7)}$$

El Niño drought-induced tropical post-fire mortality ($\boldsymbol{VC^{-}_{Mort}}$)

C_{Mort} is estimated for El Niño years only given that current data on drought induced post-fire mortality extends from these years. For this estimate we do not consider belowground mortality losses since these are not estimated in the literature for this type of disturbance event. To get the *per-PFT* total aboveground fraction of biomass allocation, we extract annual gridded biomass allocation terms and sum them over the total biomass allocated to all vegetation C pools for each PFT (fVC_{AG}^{PFT}). The approximate total above and below -ground vegetative biomass C of tropical PFTs for each gridcell and year is obtained by weighting total vegetation C per pixel (a non-PFT specific variable) by the fractional vegetation coverage of that pixel by that PFT ($fPFT_{Pix}$) and the relative NPP of that pixel versus that of the pixel mean NPP. Multiplying this by (fVC_{AG}^{PFT}) gives an estimate of the total aboveground annual biomass of the two tropical PFTs per pixel:

$$\boldsymbol{VC_{AG}^{PFT} = [VC_{Total}^{PFT} * fPFT_{Pix} * (NPP_{Pix}^{PFT}/\overline{NPP_{Pix}})] * fVC_{AG}^{PFT}} \quad \textbf{(8)}$$

Annual aboveground biomass maps are then filtered to mask out pixels where fire is absent in a given year, and filtered again to exclude non-El Niño years. El Niño years are defined here as those in which the El Niño Ocean Index >1.5 ('moderate' to 'high' intensity El Niño events). Where index values cross 1.5 for 2 consecutive years (double peak) we select both years. The resulting gridded VC_{AG}^{PFT} dataset is then used to estimate the proportion of tropical vegetation affected by fire in an El Niño year by multiplying the probability that a fire in a given pixel comes from a given PFT by the burned fraction of that PFT:

$$\boldsymbol{FireVC_{AG}^{PFT} = VC_{AG}^{PFT} * p(Fire)_{PFT} * fBurn_{Pix}} \quad \textbf{(9)}$$

To capture only those areas that may have experienced drought and hence drought induced fire mortality, we assume that drought occurs in a pixel if annual precipitation for that pixel is at or below the 25th percentile of precipitation for that pixel over the entire simulation period and mask out pixels in the dataset $FireVC_{AG}^{PFT}$ which do not satisfy this condition. We then assume that total post-fire mortality loss is approximated from the mean literature value of -24.8% (±6.9%)[19] and define this fraction as the total C-loss. However, since this biomass loss should be recoverable by the biosphere if BRI<FRI, only those pixels in which BRI>FRI are considered time-integrated losses, and only by the fraction given by the ratio of the two. Thus:

$$\boldsymbol{where\ BRI > FRI:\ VC^{-}_{Mort} = (FireVC_{AG}^{PFT} * 0.248) * (^{BRI_{PFT}}/_{FRI_{PFT}})} \quad \textbf{(10)}$$

This loss is then summed over time and annualized (divided by simulation length (yrs) to derive an annual-equivalent loss of biomass C from non-recoverable tropical forest mortality.

Soil carbon loss in areas with high frequency fire ($\boldsymbol{SOC^{-}_{hfloss}}$)

These losses are based on a recent empirical study[20] which found that large topsoil SOC losses are apparent across multiple sites globally in areas with high fire frequency', defined therein as anywhere with roughly 4.3 times the mean fire frequency for a given vegetation type, with losses of 27% and 21% accruing in areas of broadleaf and grassland vegetation. Here, and for each PFT defined as broadleaf forest and grassland, we approximate this loss spatially first by isolating those pixels which have an FRI ≥4.3x that of the global average of that PFT (the threshold identified in ref. [20]). To account for the fact that the model simulation is transient and hence in the early years of simulation the topsoil carbon stocks will be unrealistically low, we only analyse SOC^{-}_{hfloss} for the last 30 years of simulation (1981-2010). The loss over the top 19cm of the soil column, based on the literature-derived soil loss parameters (27% ± 18% for broadleaf, 21% ± 12% for grassland)[20], is estimated for the relevant pixels during 1981-2010. Although SOC losses are not fully saturating in the Pellegrini et al. study, they are close enough that we assume that they represent total SOC losses due to high frequency fires. Our estimate is limited

because the loss term is predicated on the last 30 years of simulation, whereas FRI is based on the temporal range of the simulation (110yrs; see above). Thus, once annualised, the SOC^{-}_{hfloss} estimate is constant over the whole simulation.

PyC export losses within the inland water network (SOC^{-}_{PyCExp})

A recent study has provided the first credible estimate to show that ~18 Tg of PyC in dissolved phase (Py-DOC) flushes out of the global terrestrial landmass into the inland aquatic network annually[21], while estimates of similar particulate PyC (Py-POC) aquatic export are thought to total ~25 TgC yr^{-1} [21,22]. Here, we use ORCHIDEE-MICT to construct the first gridded, PFT-specific and spatio-temporally dynamic estimate of outflux. Jones et al. (2020) estimated that boreal, tropical (<30° N/S) and temperate regions export 3.8 (± 0.6), 12.4 (± 4.9) and 1.8 (± 0.8) Tg Py-DOC yr^{-1}, respectively, providing observational constraints on the total export of Py-DOC for latitude bins ($\sum DOC_{Bin}$).

To integrate $\sum DOC_{Bin}$ with model output we estimate the contribution of each PFT to global PyC slow and PyC passive pool distributions and in doing so estimate the relative proportion of total DOC outflow originating from fires from each of these vegetation sources ($\sum DOC^{Pool}_{PFT}$). The relative global distribution of PyC produced are extracted from simulated global PyC soil pools in 1920, to approach historical distributions of PyC production. The fraction of total PyC per PFT and per PySOC pool ($f(PyC^{Pool}_{PFT})$) is calculated globally. The PFTs in $f(PyC^{Pool}_{PFT})$ are then split into boreal, temperate and tropical categories, and their fractional contribution to PyC of each bin to PyC_{Slow}/$PyC_{Passive}$ is calculated ($f(PyC_{PFT})^{Pool}_{Bin}$). C3 grasses incorporate temperate grasslands and tundra, so are split between by [temperate:boreal] surface area at 30-50° (~66%) and 50-90° N/S (~34%). Total mean absolute DOC flux (TgC yr^{-1}) per pool and PFT ($\sum \boldsymbol{DOC^{Pool}_{PFT}}$)is given by the following equation (Table S1):

$$\sum \boldsymbol{DOC^{Pool}_{PFT}} = \boldsymbol{f(PyC^{Pool}_{PFT})} * \boldsymbol{f(PyC_{PFT})^{Pool}_{Bin}} * \sum \boldsymbol{DOC_{Bin}} \qquad \textbf{(11)}$$

We assume that Py-POC export occurs proportionally to Py-DOC export based on their literature-reported global export rates, such that total Py-POC+DOC export occurs at a rate 2.39 (= (18+25)/25) times that of Py-DOC. The total Py-SOC that is hydrologically mobilized from each soil pool ($Hyd.PyC^{Pool}_{PFT}$) is thus given by:

$$\sum \boldsymbol{Hyd.PyC^{Pool}_{PFT}} = \sum \boldsymbol{DOC^{Pool}_{PFT}} * \boldsymbol{2.388} \qquad \textbf{(12)}$$

The global export quantities are then distributed spatially over the globe in proportion to soil PyC stocks. by a weighting based on the per-pixel fraction of the summed per-pool vertical PyC profile that is constituted by that pixel ($OUT^{Pool}_{PFT,Pixel}$):

$$\boldsymbol{OUT^{Pool}_{PFT,Pixel}} = \sum \boldsymbol{DOC^{Pool}_{PFT}} / (\frac{\sum^{0m}_{3m} \boldsymbol{PyC^{Pool}_{Pix}}}{\sum^{0m}_{3m} \boldsymbol{PyC^{Pool}_{Globe}}}) \qquad \textbf{(13)}$$

This generates gridded estimates for mean annual PFT-specific DOC+POC export that are constrained by the global latitude-specific estimates reported in ref.([21]). Interannual variability is implemented by allowing export to vary for each pixel by up 25% of the central value for each pixel in a manner that scales with deviation of annual precipitation from the median of the simulation period. Uncertainty is calculated by adjusting the DOC outflow values ($\sum DOC_{Bin}$) within the uncertainty ranges reported in ([21]).

References

1. Zhu, D. *et al.* Improving the dynamics of Northern Hemisphere high-latitude vegetation in the ORCHIDEE ecosystem model. *Geosci. Model Dev.* (2015). doi:10.5194/gmd-8-2263-2015
2. Zhu, D. *et al.* Simulating soil organic carbon in yedoma deposits during the Last Glacial Maximum in a land surface model. *Geophys. Res. Lett.* **43**, 5133–5142 (2016).
3. Guimberteau, M. *et al.* ORCHIDEE-MICT (v8.4.1), a land surface model for the high latitudes: model description and validation. *Geosci. Model Dev.* **11**, 121–163 (2018).
4. Krinner, G. *et al.* A dynamic global vegetation model for studies of the coupled

atmosphere-biosphere system. *Global Biogeochem. Cycles* **19**, (2005).
5. Yue, C. *et al.* Modelling the role of fires in the terrestrial carbon balance by incorporating SPITFIRE into the global vegetation model ORCHIDEE - Part 1: Simulating historical global burned area and fire regimes. *Geosci. Model Dev.* (2014). doi:10.5194/gmd-7-2747-2014
6. Yue, C., Ciais, P., Cadule, P., Thonicke, K. & Van Leeuwen, T. T. Modelling the role of fires in the terrestrial carbon balance by incorporating SPITFIRE into the global vegetation model ORCHIDEE -Part 2: Carbon emissions and the role of fires in the global carbon balance. *Geosci. Model Dev.* (2015). doi:10.5194/gmd-8-1321-2015
7. Yue, C., Ciais, P., Cadule, P., Thonicke, K. & Van Leeuwen, T. T. Modelling the role of fires in the terrestrial carbon balance by incorporating SPITFIRE into the global vegetation model ORCHIDEE -Part 2: Carbon emissions and the role of fires in the global carbon balance. *Geosci. Model Dev.* **8**, 1321–1338 (2015).
8. Thonicke, K. *et al.* The influence of vegetation, fire spread and fire behaviour on biomass burning and trace gas emissions: Results from a process-based model. *Biogeosciences* (2010). doi:10.5194/bg-7-1991-2010
9. Hantson, S. *et al.* The status and challenge of global fire modelling. *Biogeosciences* (2016). doi:10.5194/bg-13-3359-2016
10. Hantson, S. *et al.* Quantitative assessment of fire and vegetation properties in simulations with fire-enabled vegetation models from the Fire Model Intercomparison Project. *Geosci. Model Dev.* (2020). doi:10.5194/gmd-13-3299-2020
11. Li, F. *et al.* Historical (1700-2012) global multi-model estimates of the fire emissions from the Fire Modeling Intercomparison Project (FireMIP). *Atmos. Chem. Phys.* (2019). doi:10.5194/acp-19-12545-2019
12. Van Marle, M. J. E. *et al.* Historic global biomass burning emissions for CMIP6 (BB4CMIP) based on merging satellite observations with proxies and fire models (1750-2015). *Geoscientific Model Development* (2017). doi:10.5194/gmd-10-3329-2017
13. Forkel, M. *et al.* Emergent relationships with respect to burned area in global satellite observations and fire-enabled vegetation models. *Biogeosciences* (2019). doi:10.5194/bg-16-57-2019
14. Jones, M. W., Santín, C., van der Werf, G. R. & Doerr, S. H. Global fire emissions buffered by the production of pyrogenic carbon. *Nat. Geosci.* (2019). doi:10.1038/s41561-019-0403-x
15. Parton, W. J., Stewart, J. W. B. & Cole, C. V. Dynamics of C, N, P and S in grassland soils: a model. *Biogeochemistry* (1988). doi:10.1007/BF02180320
16. Singh, N. *et al.* Transformation and stabilization of pyrogenic organic matter in a temperate forest field experiment. *Glob. Chang. Biol.* (2014). doi:10.1111/gcb.12459
17. Viovy, N. CRUNCEP Version 7 - Atmospheric Forcing Data for the Community Land Model. *Research Data Archive at the National Center for Atmospheric Research, Computational and Information Systems Laboratory* (2018). doi:https://doi.org/10.5065/PZ8F-F017. Accessed 22/02/2020
18. Fu, Z. *et al.* Recovery time and state change of terrestrial carbon cycle after disturbance. *Environ. Res. Lett.* (2017). doi:10.1088/1748-9326/aa8a5c
19. Silva, C. V. J. *et al.* Drought-induced Amazonian wildfires instigate a decadal-scale disruption of forest carbon dynamics. *Philos. Trans. R. Soc. B Biol. Sci.* (2018). doi:10.1098/rstb.2018.0043
20. Pellegrini, A. F. A. *et al.* Fire frequency drives decadal changes in soil carbon and nitrogen and ecosystem productivity. *Nature* **553**, (2018).
21. Jones, M. W. *et al.* Fires prime terrestrial organic carbon for riverine export to the

global oceans. *Nat. Commun.* (2020). doi:10.1038/s41467-020-16576-z
22. Coppola, A. I. *et al.* Global-scale evidence for the refractory nature of riverine black carbon. *Nat. Geosci.* (2018). doi:10.1038/s41561-018-0159-8

Figures

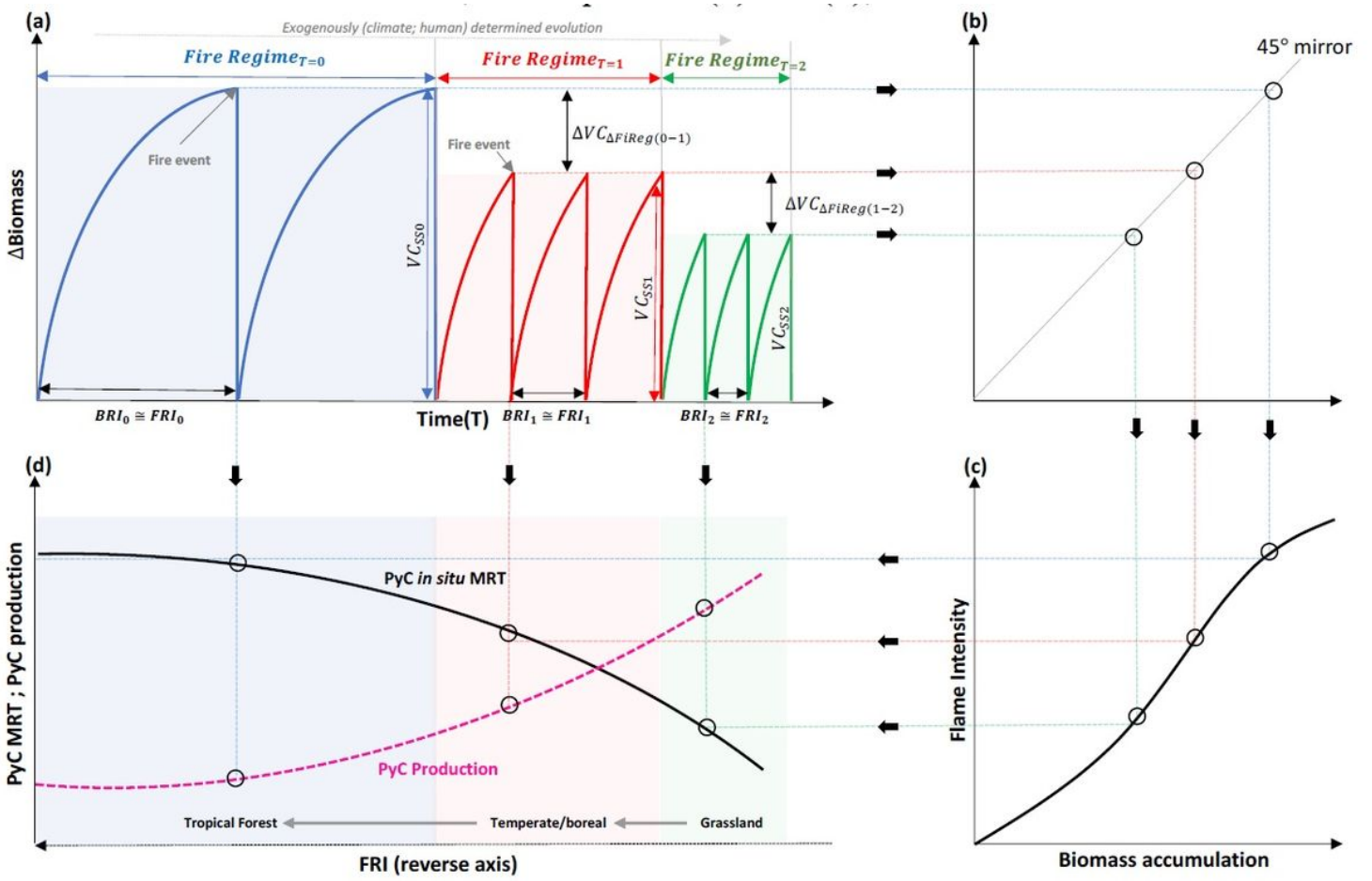

Figure 1

Schematic representation of the interrelation between plot or biome -scale. (see full caption in Manuscript file)

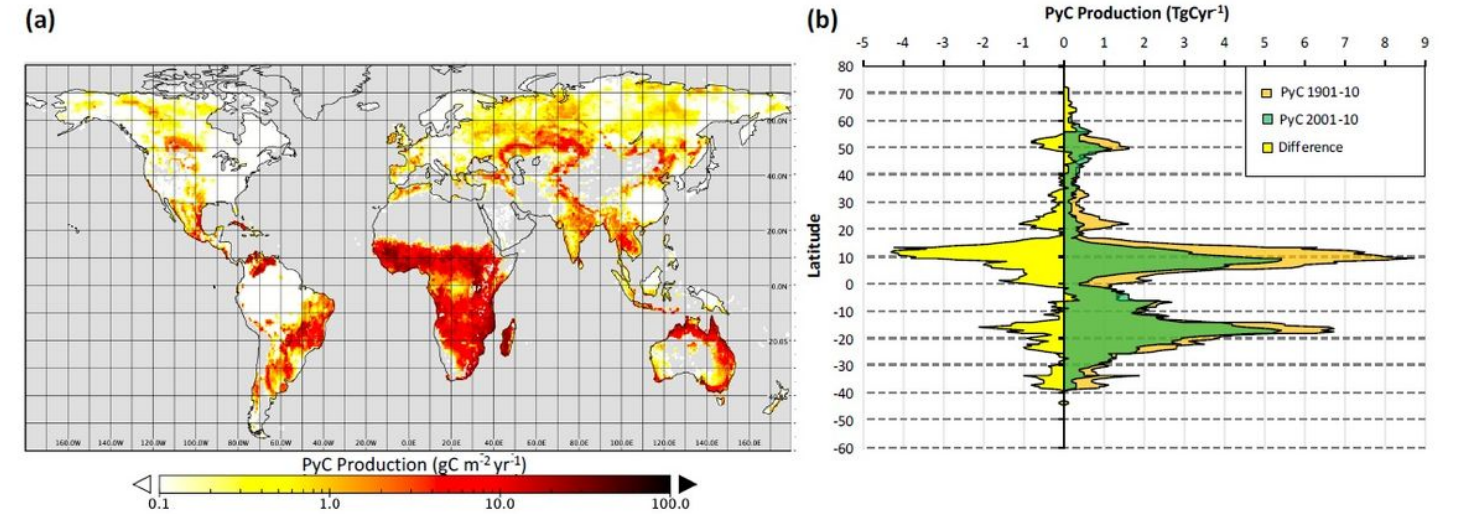

Figure 2

Simulated PyC production and change over 1901-2010. (a) Map 130 of global PyC production averaged over the entire simulation period (log gC m-2yr-1). (b) Simulation-averaged annual absolute PyC production summed per 0.5° latitude bin (TgC yr-1) in 1901-10 (orange) and 2001-10 (green), with the difference (latter-former) shown in yellow. Note: The designations employed and the presentation of the material on this map do not imply the expression of any opinion whatsoever on the part of Research Square concerning the legal status of any country, territory, city or area or of its authorities, or concerning the delimitation of its frontiers or boundaries. This map has been provided by the authors.

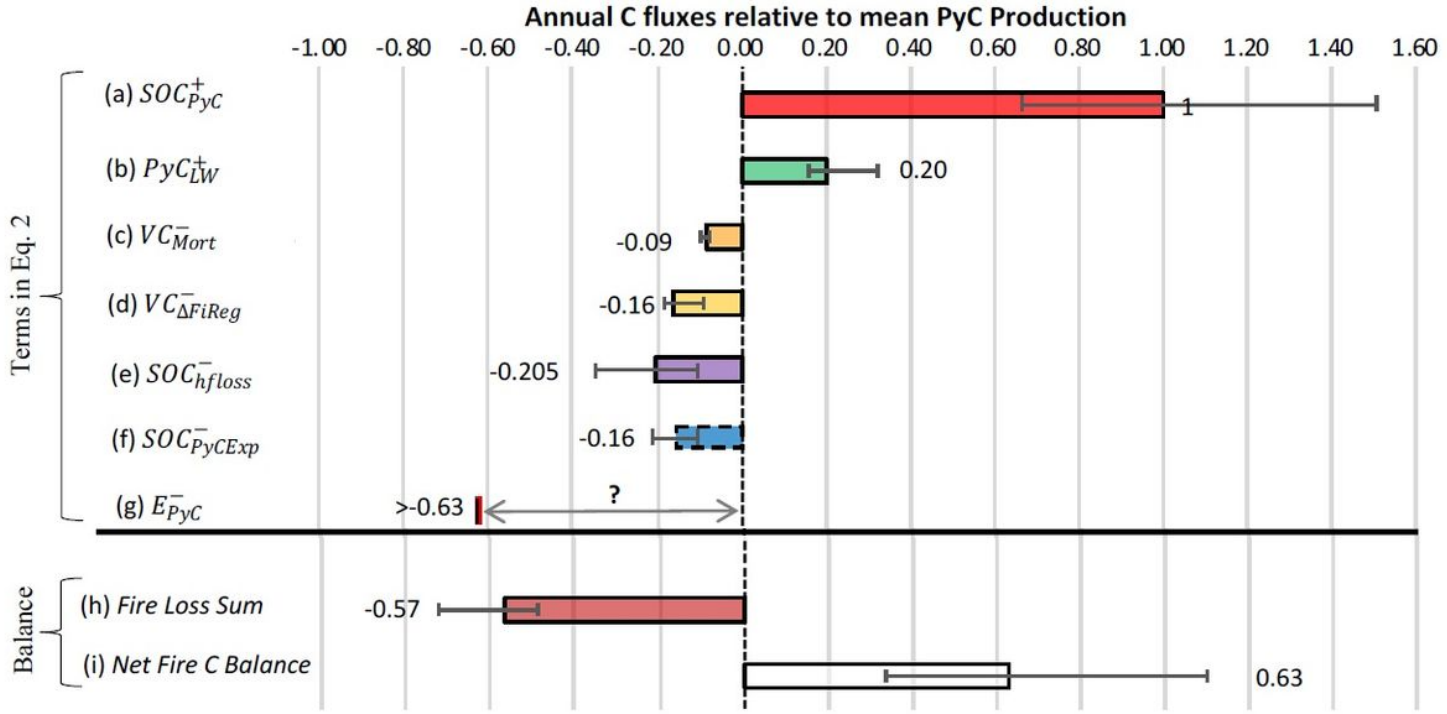

Figure 3

Time averaged estimates for the source and sink terms in Eq. 2 .(see full caption in Manuscript file)

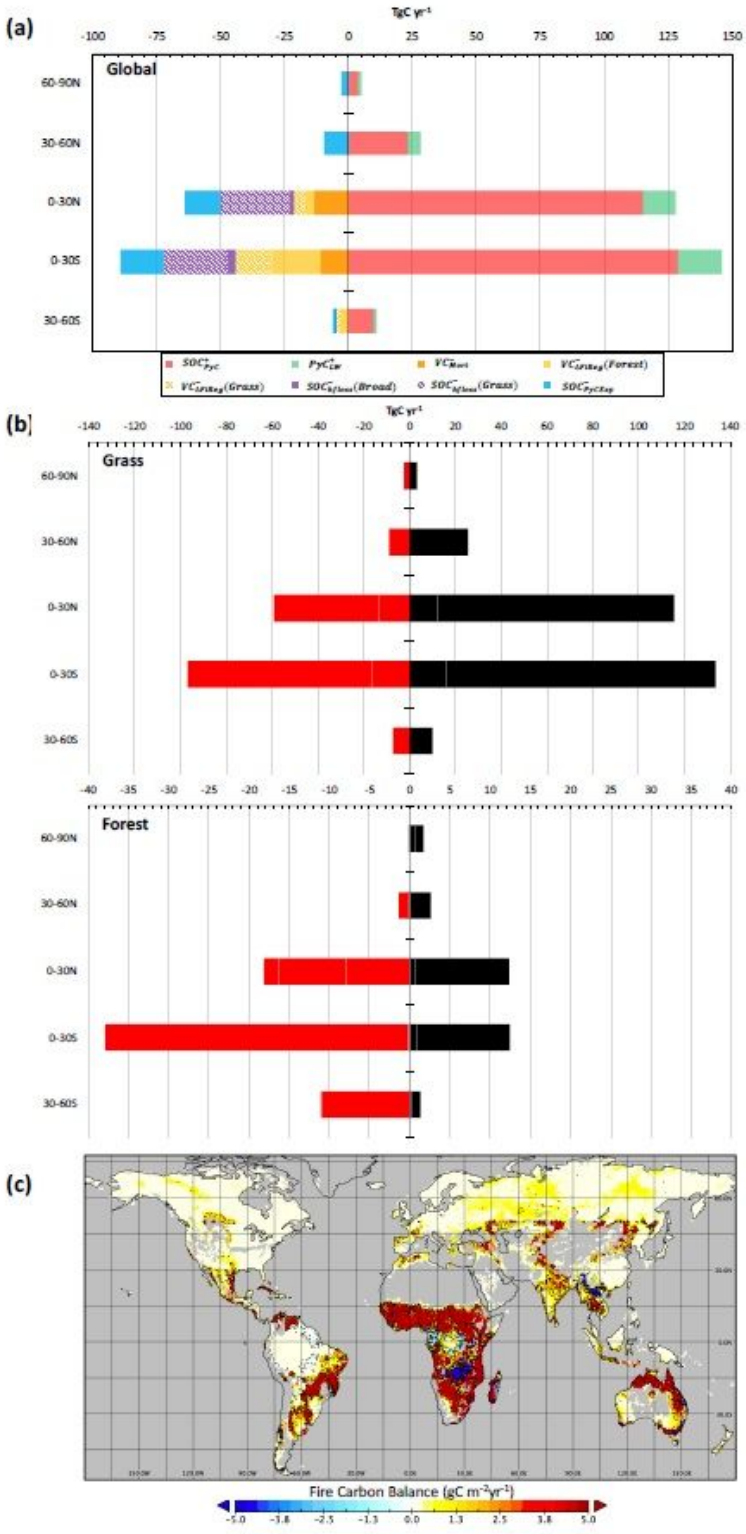

Figure 4

Global fire C-248 cycle. (see full caption in Manuscript file) Note: The designations employed and the presentation of the material on this map do not imply the expression of any opinion whatsoever on the part of Research Square concerning the legal status of any country, territory, city or area or of its authorities, or concerning the delimitation of its frontiers or boundaries. This map has been provided by the authors.

Supplementary Files

This is a list of supplementary files associated with this preprint. Click to download.

- M1FireCarbonBalanceFinalDraftSupplement.pdf